Methyl-ammonium lead iodide hybrid perovskite thin film as active material for energy conversion devices

J. Chaudhary[a], R. Agrawal[b], D. Kumar[c], S. K. Pathak[d], M. Chandra[e], S. Kumar[f], A. S. Verma[g,h,*]

[a]*Department of Physical Sciences, Banasthali Vidyapith, Banasthali 304022 India*
[b]*Department of Computer Engineering and Applications, G. L. A. University Mathura 281406 India*
[c]*Department of Chemical Engineering, Banasthali Vidyapith, Banasthali 304022 India*
[d]*Department of Physics, Chintamani College of Science, Pombhurna, Chandrapur, Maharashtra 442918 India*
[e]*Department of Physics, Poornima Institute of Engineering & Technology, Jaipur 302022 India*
[f]*Department of Chemistry, Banasthali Vidyapith, Banasthali 304022 India*
[g]*Division of Research & Innovation, School of Applied and Life Sciences, Uttaranchal University, Dehradun, Uttarakhand 284007 India*
[h]*University Centre for Research & Development, Department of Physics, Chandigarh University, Mohali, Punjab 140413 India*

The use of hybrid halide Perovskites is helping us get closer to our aim of completely self-sufficient structures in terms of energy production. Preparation of a device of photoactive material $CH_3NH_3PbI_3$ {FTO (Fluorine-doped tin Oxide)/ $CH_3NH_3PbI_3$/Spiro-OMeTAD/Al} for the photovoltaic applications has been described in this article. Producing a homogeneous thin film through the use of lower temperature, processed-solution devices with one-step spin coating processes is an essential stage in the fabrication process. To generate the thin films on the FTO-substrate, the one-step spin coating approach was utilized for the deposition of the precursor solution, which consisted of methylammonium iodide and lead iodide in a molar ratio of 3:1. This technique was employed to prepare the thin films. The FESEM technique was utilized to carry out the investigation of the surface morphology of this thin layer. In addition, the essential parameters of this device, like barrier height, saturation current, current density, ideality factor, carrier mobility, resistance, carrier lifetime, and capacitance have been computed using current-voltage (I-V) characteristics and the impedance spectroscopy technique. A laser with a power of 20 milliwatts and a wavelength of 532 nanometers was used to light the gadget. The current conduction mechanism exhibits ohmic behavior at a low voltage, while at medium voltages, TFSCLC is the mechanism that regulates charge transportation. Despite the fact that TCSCLC is demonstrated at higher voltages. The TCSCLC model was used to conduct an investigation of the hole's mobility.

(Received August 1, 2023; Accepted April 8, 2024)

Keywords: Hybrid perovskites, Charge carrier mobility, Electrochemical impedance spectroscopy, Life-time

1. Introduction

Electronic organic devices present a viable option for renewable sources of power and various additional uses for the ease with which they may be produced, the simplicity of the required components, and the negligible impact they have on the environment [1]. A significant amount of investigation has been concentrated on the development of innovative and feasible non-

* Corresponding author: ajay_phy@rediffmail.com
https://doi.org/10.15251/JOR.2024.202.233

silicon solar cell technologies. Halide perovskites have evolved with remarkable efficiency of 22.7% in terms of barely any years as a capability of this invention for alternative energy [2]. Research that is still being compiled shows that productivity in the power transformation industry has increased rapidly, moving from 3.8% in 2009 to 24.2% in 2019 [3]. Materials with an organic-inorganic hybrid structure that are based on photovoltaic cells have demonstrated a level of perfection that stands in stark contrast to that of existing inorganic semiconductor developments or silicon-based technology. This can be seen in areas such as production costs, adaptability, and assembly requirements [4]. Therefore, this way perovskite-based optoelectronic devices have attracted a unique approach of reestablished attempts at mounting the highest possible level of efficiency [5]. The primary 3D perovskite producers have been accounted for in permeable structure in $CH_3NH_3PbX_3$ nanoparticles (NPs), and as a consequence the extent of perovskites as producers uncovered [6]. As a result, the investigation into the manufacturers of 3D perovskites has become much more advanced and concentrated on the achievement of high levels of competency in photoluminescence and electroluminescence [7]. Without a doubt, there are remunerated striking endeavors through the analysts to examine the opening obstructing material (HBM) or opening vehicle materials (HTL). Subsequently, in this study, it was strongly implied that the electron transport materials might not be sufficient to achieve a higher efficacy. In spite of this, Spiro-OMeTAD plays a significant part in perovskite-based devices ability to block electrons, transport holes, and impede the recombination of charges. Furthermore, to improve this opening shipping materials which are useful to upgrade the presentation of perovskite-based solar cells [8-16].

A wide variety of strategies have been utilized to shape uniform perovskite film, including turn covering, dip coating, thermal evaporation, spray coating and vapor facilitated technology [17-21]. The semiconducting way of hybrid halide perovskite-based devices minority-transporter diffusion lengths and high transporter mobility are required for both charge transport and resistivity to be achieved. In addition, ionic charge transport in hybrid perovskites may be able to be observed through the use of impedance spectroscopy for research [22].

The $CH_3NH_3PbI_3$ is a suitable contender to be utilized as an active layer in optoelectronics gadgets. The function of the sensitizer in these hybrid perovskite nanoparticles is to embeddings, electrons in the ETLs and holes in the HTLs, and together the layers are utilized as particular interacts all throughout; which the charge transporters designed by photograph excitation in the device [23, 24].

Various HTLs like as P3HT: PCBM, PEDOT: PSS, and Spiro-OMeTAD are accounted for. In the present research, we have made use of Spiro-OMeTAD as a HTL material. This material was sandwiched within the perovskite layer and the dissipated metal cathode. Powerful masses of photo-generated holes and electrons have detailed; mass of electrons $m_e^* = 0.23\ m_o$ and mass of holes $m_h^* = 0.29\ m_o$, separately [25].

The constituents that will make up the transport layers are selected with the objective of the energy impediments having to anticipate the passage of holes into the ETL and electrons into the HTL in mind when the materials are selected. The performance of solar-based cells is improved by using Spiro-OMeTAD as HTL [26-29].

The compelling charge transporter flexibility is often reliant on the diffusion length of the cell and, as a result, the opportunity for an energized charge transporter to reach their respective cathodes. At the end of the day, it is possible that leaks in the precious stone structure will shorten the lifespan of the photograph created charge transporters in the device [30-32]. Impedance spectroscopy (IS), has seen widespread use in recent years for the purpose of analyzing the design specifications of natural photovoltaic devices. In this article, we will discuss the fundamental approach to dealing with the study of impedance spectroscopy applying tantamount circuit analysis. It is necessary to have an in-depth understanding of the operational parameters of this solar device in order to facilitate the streamlining and further development of another photovoltaic invention [33-35].

2. Details of experiment

2.1. Used materials for fabrication of device

FTO glass substrate, Methylamine (CH_3NH_2), HI (hydriodic acid) and 2,2',7,7'- Tetrakis [N, N-di (4-methoxyphenyl) amino]-9,9'- spirobifluorene (Spiro-OMeTAD) were purchased from Sigma Aldrich, while dissoluble anhydrous N, N-dimethyl-formamide (DMF) and aprotic dissolvable diethyl ether was purchased from Merck. Every one of these components was used in its raw form, without any extra sorting or cleaning being done.

2.2. Ozone treatment for cleaning of substrate:

FTO substrates were washed with Lebolene soap, after which it is successively cleaned by using distilled water, acetone and 2-propanol for 15 minutes in an ultrasonic bath. Subsequently, the substrate was exposed to UV light for 15 minutes in order to enhance the surface grip of the substrate, which in turn enhanced the performance of the device.

2.3. Synthesis of $CH_3NH_3PbI_3$ perovskite precursor solution:

The production of the perovskite precursor has been broken down into its component parts and presented in the following diagram:

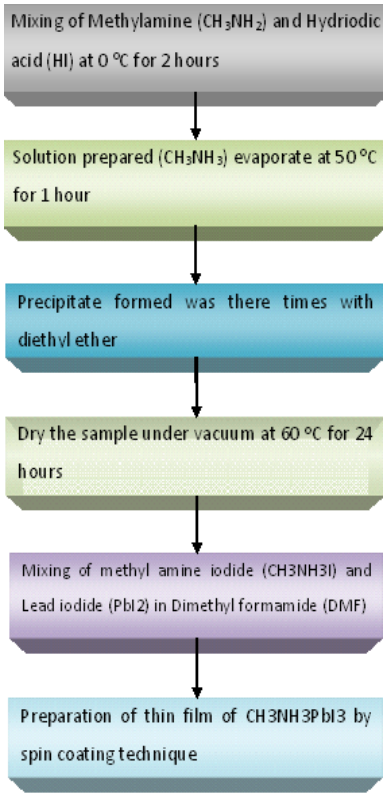

Fig. 1. Procedure for the synthesis of perovskite precursor solution.

In the preparation of methyl amine lead iodide ($CH_3NH_3PbI_3$), the following reactions are involved.

$$CH_3NH_2 + HI \rightarrow CH_3NH_3 + I$$

$$CH_3NH_3I + PbI_2 \rightarrow CH_3NH_3PbI_3$$

In the presence of CH_3NH_3I and PbI_2 in (3:1), pale yellow solution is obtained, since solubility of PbI2 is recognized to be enhanced in DMF in the presence of CH_3NH_3I. In order to get the transparent yellow solution prior to spin coating, the solution should be heated to 70 ^{0}C for

up to 30 minutes while being vigorously stirred. It is possible that a smooth film cannot be obtained due to the presence of white residues in the solution.

2.4. Device fabrication and characterization

The spin coating technique was used to store the obtained perovskite solution onto the glass substrate. The surface morphology of the generated perovskite nanoparticles is illustrated in figure 2 (a) and (b). Preparation of perovskite-based devices (perovskite/FTO/Spiro-OMeTAD/Al) are represented in figure 3 (a, b). In the first step of the manufacturing process for a perovskite-based device, a perovskite solution was spin-coated onto a fluorine-doped oxide glass substrate at a speed of 2000 rpm for 40 seconds. This was done using a one-step spin coating method to form the photon-absorbing layer. Afterward the substrate was reinforced at 70° C for 5 minutes. The HTL of Spiro-OMeTAD coated over perovskite active layer at 3000 rpm for 40 seconds by spin coating method. The active perovskite layer as well as the hole transport layer were both deposited in a glove box unit or in an environment that was completely inert. Lastly, in order to complete the formation of the device's top electrode, aluminium in the shape of an electrode was deposited onto the HTL using the process of thermal evaporation at a pressure of 10-5 torr. Presently, the manufactured device has been done for additional characterization using different procedures.

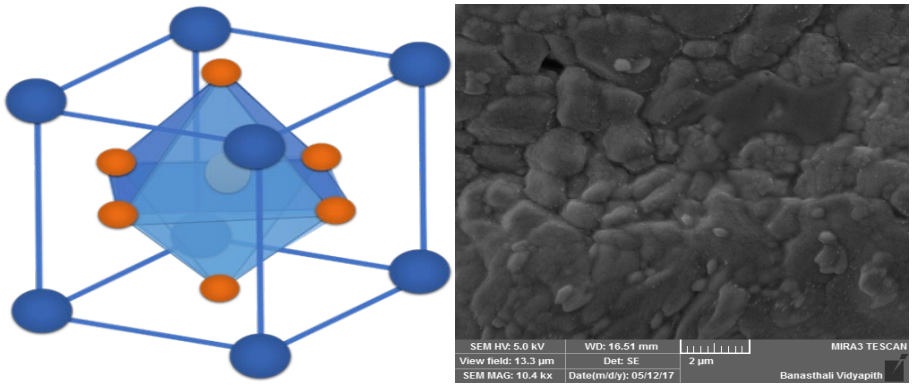

(a) *(b)*

Fig. 2. Morphology of perovskite thin film accumulated onto glass-substrate; (a) Crystal Structure of Perovskite, (b) FESEM image of $CH_3NH_3PbI_3$ perovskite thin film.

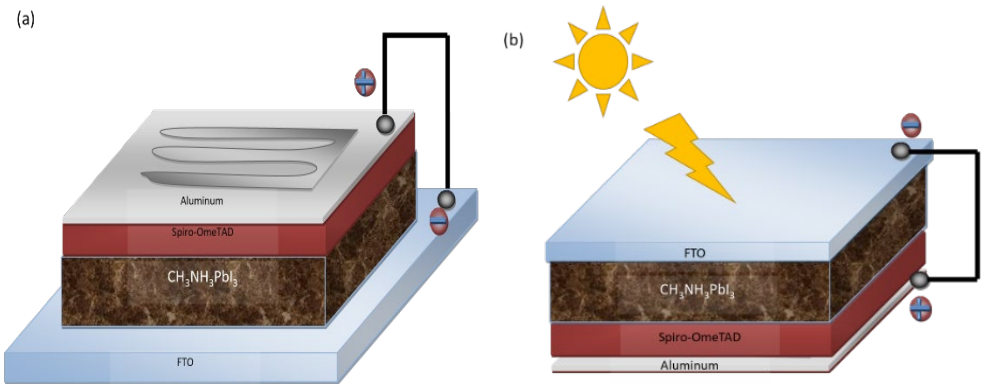

Fig. 3. (a, b) Heterostructure of the device structure with the active layer of perovskite.

2.5. Techniques for characterization

The surface morphology of the $CH_3NH_3PbI_3$ thin film has procured utilizing FESEM (Tescan MIRA 3 LMU FEG). The (I–V) evaluations were taken by the assistance of a Keithley source meter 2612 appended with a manual test station (LA-100 DC, Semi-test USA). Electrochemical impedance spectroscopy was utilized so that the device's internal electrical characteristics could be determined and characterized (EIS). The impedance spectrum of the device was procured utilizing an electrochemical workstation (Auto lab PGSTAT30) at 0 V in obscurity. The EIS-analyzer programming was applied so that the findings of the EIS could be fitted and investigated.

3. Results and discussion

We have investigated in this article about the photoactive material execution of methylammonium lead iodide base device (FTO/$CH_3NH_3PbI_3$/Spiro-OMeTAD/Al). The quality of the film is the first stage, and it is primarily responsible for determining the dexterous boundaries of the device. The comprehensive surface inclusion of thin film expansion onto substrate of glass with the grains of the perovskite crystal has been portrayed by FESEM; as appeared in figure 2. As a result, we have analyzed from figure 2 (b) that $CH_3NH_3PbI_3$ perovskite thin film can be developed by uniform grains, total surface inclusion and immaterial agglomeration. Under both dark and light conditions, the device's (I-V) characteristics were analyzed and compared. The device was illuminated from FTO side using a laser of intensity 20mW working at frequency of 532nm. In the preceding I-V curve, the exceptional dependency of forward current on voltage as well as saturation current in the reverse bias state indicates the shifting behaviour of the device. The voltage application in forward bias reduces the infusion blockage for holes and electrons, as represented by energy band diagram 3(c). Figure 3 (a, b) displays the heterostructure of the constructed device, coupled using the probable transportation of the photo-generated charge-carrier, which is depicted in the energy band diagram, figure 3 (b).

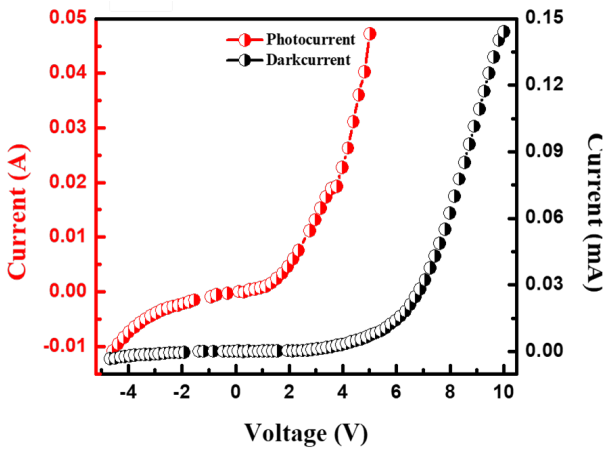

Fig. 4. I-V curve of the $CH_3NH_3PbI_3$ device in dark and illumination.

As indicated the (I-V) characteristics of the photoactive (FTO/$CH_3NH_3PbI_3$/ Spiro-OMeTAD/Al) device under dark and enlightenment as expressed in figure 4. The forward bias of the I-V curve results in a significant increase in the current in both the dark and the light conditions. Despite this, there is less of an impediment to the flow of energy. This is because the imbalance in the device's internal field has been corrected, and the bands have become more uniform. As a result, charge carriers (electrons and holes) are able to flow more freely toward their respective cathodes (FTO/Al). Also, under reverse bias, the charge carriers face endures in transportation in light of the fact that the Fermi level splitting and energy obstruction turns out to be high of 1.5eV at the interfaces of Al/Spiro-OMeTAD due to which the electrons can't move as quick as they move in forward inclination.

Accordingly, this is the manifestation of electron blocking interface, and in the same way, holes injection blocks are brought about by the high energy barrier of 2.1 eV at the interface of FTO/perovskite, which brings about a limited current flow in the opposite direction. In addition to this, it has become abundantly evident that exciting a device with light causes significant variations in the current levels, which improve by increasing the voltage that is applied. Excitons were generated in the active layer of the device whenever the light was turned on. The formation of an electric field and the application of an external voltage were subsequently utilized in order to separate these excitons into their constituent free charge carriers, which were holes and electrons.

These free charge carriers then affected by applied voltage were shifted to the terminals (cathode and anode) as figure 3 (b), an appropriate photocurrent appeared in device FTO/$CH_3NH_3PbI_3$/ Spiro-OMeTAD/Al as depicted by Figure 4. This considerable change in the photocurrent has almost completely been due to the higher charge collecting productivity. In the presence of light, photons of various energies are absorbed by the perovskite layer, which results in the production of the highest number of excitons. Excitons are subjected to an energy process that leads them to decompose into the individual free charge carriers that make up their component bands, like holes present in the valence band and electrons present in the conduction band.

The photoexcited holes go in the direction of the HTL (Spiro-OMeTAD), where they are eventually collected by the Al cathode. In contrast, the photo-electrode (FTO) has an effect on the movement of the electrons, which cause them to move in response to an applied electric field. As a result, there is a rise in the photocurrent on reverse bias. Spiro-OMeTAD continues to be the standard HTM and has been presented as a potential material as the hole transport layer in perovskite-based devices; as a result, it is receiving significant consideration in this area. In any event, this material has persistently shown the suitable coordinating of HOMO-LUMO levels using the perovskite material, that is added to increase the photocurrent in the perovskite-based devices. The photovoltaic performance of perovskite ($CH_3NH_3PbI_3$) crystals has been significantly enhanced by increasing the temperature in which methyl amine iodide has been dried throughout the combination of methylamine arrangement, and further expand the boundaries, such as saturation current (Is), trap density, hole's mobility, detectivity, and barrier height, as a result of carrier diffusion, progression of charge generation, and separation of charge in the device. Table 1 provides a summary of the data on the impact of structural boundaries, as applied from I-V estimates of the devices, on photocurrent.

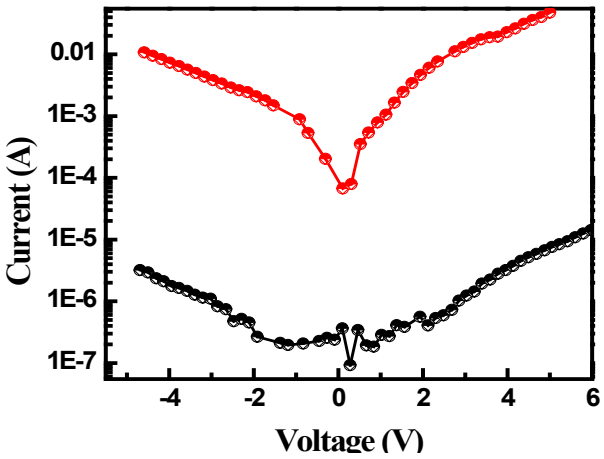

Fig. 5. I-V black curve illustrations semi-logarithmic curve with $CH_3NH_3PbI_3$ device.

Table 1. Device parameter and values.

Parameter	**Values**
I_S (Amp)-dark	1.15×10^{-6}
I_S (Amp)-light	3.38×10^{-4}
Detectivity (Jones)	1.09×10^{12}
Barrier height ϕ_B (Volt)-dark	0.85
Barrier height ϕ_B (Volt)-light	0.71
Electron Mobility μ ($cm^2v^{-1}s^{-1}$)	9.01×10^{-5}
Trap density n_t (cm^3)	1.20×10^{16}

It was found that the device is able to handle appropriate currents, as stated in table 1; the reverse saturation current (Is) was extracted using the Shockley diode equation [36], and the semi-logarithmic plot of the I-V curve at 0 V is depicted in figure 5:

$$I = I_s\left[\exp\left(\frac{qV}{\eta kT}\right) - 1\right] \quad (1)$$

where, e is the electronic charge, k means Boltzmann's constant, η indicates to the ideality factor of diode, T is absolute temperature, V is the applied voltage, and I_s indicates reverse saturation current. Consequently, the ideality factor and the reverse saturation current may be evaluated independently on the semi-logarithmic I-V characteristics curve using the slope and the intercept at the y axis at 0 V. This information is derived from the information on Is. The ideality factor value that is close to 1 indicates a Schottky diode or an ideal diode, and the ideality factor value that is more than 1 indicates that the current grows at a more gradual rate in contrast with η=1. Due to the existence of interface states, traps, and barrier inhomogeneity, it is possible that high estimates of η for the manufactured device will result from increased recombination. Nevertheless, the Schottky diode border is governed by the barrier height (ϕ_B), which is described by the following relation [37].

$$I_s = AA^*T^2\exp\left(-\frac{q\phi_B}{kT}\right) \quad (2)$$

Here A represents area and A^* is the Richardson's constant.

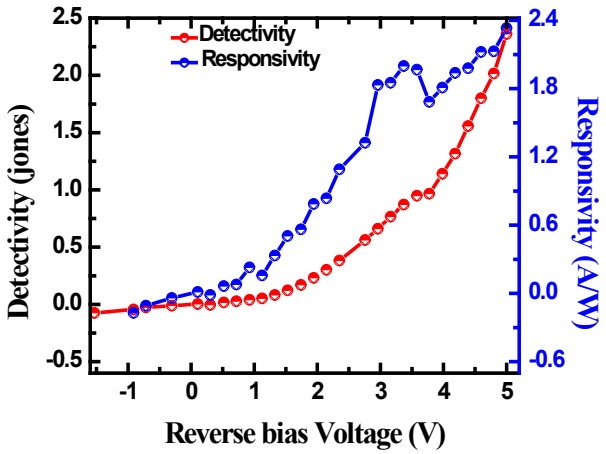

Fig. 6. Fabricated device responsivity and detectivity.

The standard diode or photodetector have been shows different significant boundaries; responsivity and detectivity are two of them. The ratio of the produced photocurrent (Iph) to the amount of optical power (PO) that occurs on the detector has been used to assess the detector's responsivity, and this ratio is then utilized in the following equation to estimate the detector's responsiveness [38]:

$$R_P = \frac{I_{Ph}}{P_0} \quad (3)$$

Here, I_{Ph} is the photocurrent, and Po is incident optical power. Detectivity is determined by the detector's responsivity as well as its commotion comparable power; it provides an assessment of the detector's performance in relation to noise [39]. Whenever there is an excessively large quantity of shot noise in relation to the commotion source in the dark current, and the simple technique has been used to calculate the value of detectivity [40].

$$D^{*} = \frac{R_P}{(2eI_D)^{1/2}} \tag{4}$$

Here, dark current has denoted by I_D, e is the charge of electrons and R_P is responsivity.

The expected characteristics of responsivity and detectivity have been shown in figure 6 for the device on applied reverse voltage. Finally, the detectivity of device estimated at 0V was 1.09×10^{12} Jones. After that, the device demonstrated that the proper evaluation of detectability is a result of the improvement in photocurrent. Despite this, it was discovered at the event that the device has the ability to be self-powered. This is despite the fact that the gadget needs electricity from an external source in order to recognize optical signals. Within this research, the HTL is expressed to the hole extraction contact at the interface between the Spiro-OMeTAD and the active layer (the perovskite layer) in the planar photoactive device. The perovskite layer is responsible for the photoelectric effect. This makes it profoundly alluring in the photovoltaic group due to the powerful performance it possesses.

Perovskite layer's essential surface shape is capable of achieving an increase in hole mobility, which is a desirable property. In addition, by analyzing the twofold logarithmic current-voltage characteristics, which can be seen in figure 7, three distinct charge transport methods of the device have been taken into consideration. Which notice the complete power law dependency of $J \alpha V^{m}$ in such a way that m refers to the slope of the curve

As we have found in figure 7, the curve starts following the Ohmic behavior (m=1), at low voltage values. After that, the slope changes to a 2, which indicates that the TFSCLC mechanism controls the charge transport process that results in an increased voltage. As a consequence of this, the slope is now significantly greater than 3.5 (>2) as a result of the continued injection of charge carriers. As a consequence of this, the current in this region increased gradually in response to the applied voltage and followed a mechanism that was controlled by a trap charge's limited conduction capabilities (TCLC).

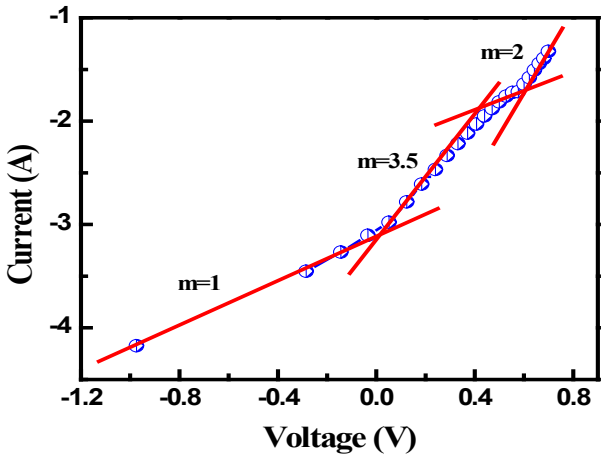

Fig. 7. Double-logarithmic plots of the devices in dark and the slope indicated by m in various regions of $CH_3NH_3PbI_3$ perovskite-based device.

This is feasible as a result of the filled traps operating at a higher voltage; hence, the traps have no effect on the current. Applying the Mott-Gurney law allows for the calculation of the hole's mobility (μ) in this area (TFSCLC) [41].

$$J_{SCLC} = \frac{9}{8}\varepsilon\varepsilon_0\mu\frac{V^2}{d^3} \tag{5}$$

where, μ represents mobility, ε denotes relative dielectric constant, ε_0 is vacuum permittivity, L denotes perovskite layer thickness and N_T is trap density that resulting in the following formula [42, 43].

$$V_{TFL} = \frac{e\, N_T\, L^2}{2\varepsilon\varepsilon_0} \tag{6}$$

where,

- L = perovskite layer thickness
- V_{TFL} = trap filled limited voltage
- N_T =trap density
- ε = dielectric constant
- ε_0 is vacuum permittivity

When the voltage was supplied to the devices, the density, electric field and charge mobility all increased, despite the fact that there were still some slight variations. As shown in table 1, the saturation current(I_s) measured in dark and light from 1.15×10^{-6} mA to 3.38×10^{-4} Amp in reverse bias direction. Accordingly, considerable changes have been made to the other characteristics in the light compared to the dark. Studying the charge transport and photo response of the manufactured device has made it abundantly evident that the device demonstrates the required characteristics, as shown by the figure and table.

The impedance spectrum analysis that has been recorded using Nyquist plots in figure 8 has been done so in order to accomplish a considerable approach nearer for the process of charge transport and interfacial charge transfer. Henceforth, the electrical equivalent circuit model shows in figure 8 (b) that gives the appropriate of the test information to take out the parameters. R_s and R_p resistances of series and parallel that used to contacts, wire and other accessories connected with the interface charge transportation process taking place within the device, while CPE is utilized as a substitute of the capacitor in the device for the quality of the better fit.

This is supplanted to Cp that has been estimated by the tailored spectrum of the device. The electrical parameters that deliberate by the built-in data of impedance spectra has appeared in table 2. Rs denote to the recombination resistance and CPE records to the coupled compound capacitance (Cμ) in manufactured device [44]. As per table 2, the estimations of CPE, R_P, and τ_n of $CH_3NH_3PbI_3$ material might be utilized as a functioning layer than the other material in the represented devices and the improvement in CPE is demonstrating to permit simple charge transport from the cathode to the active layer, in addition, increase in τ_n likewise indicates less incessant recombination. The estimation of electron life time (τ_n) is estimated by the accompanying equation [45].

$$\tau_n = R \times C \tag{5}$$

Here,

C = Capacitance determined from the simulated circuit using EIS analyzer software

R = Parallel resistance

τ_n = Life time of charge carrier's excitons emitted by the perovskite when exposed to light.

The characteristics of impedance spectra at a lower frequency are related to the electronic charge transportation qualities, whereas the features of impedance spectra at high frequency are assigned to the charge recombination component.

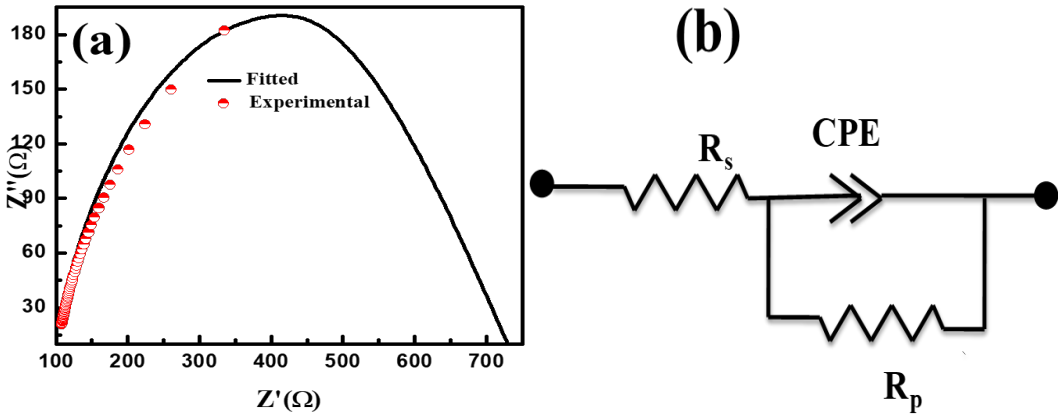

Fig. 8. (a) Nyquist plot of the employed device using $CH_3NH_3PbI_3$, and (b) electrical circuit diagram of the equivalent devices.

Table 2. The extracted and evaluated internal device parameters of the perovskite-based devices.

Parameter	$R_s(\Omega)$	$R_P(\Omega)$	CPE	τ_n (Sec.)
Values	77.42	661.96	2.48×10^{-6}	1.6×10^{-4}

4. Conclusions

We examined the electrical parameters of $CH_3NH_3PbI_3$ (FTO/$CH_3NH_3PbI_3$/Spiro-OMeTAD/Al) based device. The device was manufactured using the spin coating process, which was then applied onto an FTO-covered glass substrate that had been prepared using ultraviolet (UV) and ozone. This gives the device an advantage in terms of charge separation and lowers the recombination rates. Perovskite and the top electrode are layered within a hole transport layer and an electron blocking layer that are provided by the Spiro-OMeTAD for the purpose of achieving outstanding performance and advancing the improvement of photocurrent. The TFSCLC model was used to the constructed device in order to evaluate the charge carrier mobility of holes. The Mott-Gurney law was also utilized in this process. In addition to that, device has shown appropriate detectivity of 1.09×10^{12} Jones. Subsequently, the electrical performances of the device were investigated using I-V curves and impedance spectroscopy, and it was discovered that $CH_3NH_3PbI_3$ is an acceptable photo active material for use in photovoltaic devices. With the steady development of hybrid perovskite materials, photovoltaic innovations that are good for the environment, work well, and cost less will be used in perovskite-based photovoltaic devices all over the world in the coming years.

References

[1] J. Chaudhary, R. Gautam, S. Choudhary, A. S. Verma, European Physical Journal Applied Physics, 88, 30101 (2019); https://doi.org/10.1051/epjap/2019190023

[2] J. Chaudhary, S. Choudhary, B. Agrawal, A. S. Verma, Semiconductors, 54, 1023-1031 (2020); https://doi.org/10.1134/S1063782620090055

[3] S Choudhary, A Shukla, J Chaudhary, A. S. Verma, International Journal of Energy Research 44, 11614-11628 (2020); https://doi.org/10.1002/er.5786

[4] S. Tombe, G. Adam, H. Heilbrunner, D. H. Apaydin, C. Ulbricht, N. S. Sariciftci, C. J. Arendse, E. Iwuohaa and M. C. Scharber, J. Materials Chemistry C, 5, 1714 (2017); https://doi.org/10.1039/C6TC04830G

[5] K. Chen, S. Schünemann, S. Song, and H. Tüysüz, Chemical Society Reviews, 47, 7045

(2018); https://doi.org/10.1039/C8CS00212F

[6] A. Cannavale, P. Cossari, G. E. Eperon, S. Colella, F. Fiorito, G. Gigli, H. J. Snaith and A. Listorti, Energy & Environmental Science, 9, 2682 (2016); https://doi.org/10.1039/C6EE01514J

[7] S. T. Ha, R. Su, J. Xing, Q. Zhang, and Q. Xiong, Chemical Science, 8, 2522 (2017); https://doi.org/10.1039/C6SC04474C

[8] A. Mutalikdesai, A., and S. K. Ramasesha, Resonance, 22, 1061 (2017); https://doi.org/10.1007/s12045-017-0571-1

[9] J Burschka, N. Pellet, S. J. Moon, R. H. Baker, P. Gao, M. K. Nazeeruddin and M. Grätzel, Nature, 499, 316 (2013); https://doi.org/10.1038/nature12340

[10] H. Tan, A. Jain, O. Voznyy, X. Lan, F. P. G. D. Arquer, J. Z. Fan, R. Q. Bermudez, M. Yuan, B. Zhang, Y. Zhao, F. Fan, P. Li, L. N. Quan, Y. Zhao, Z. H. Lu, Z. Yang, S. Hoogland, and E. H. Sargent, Science, 355, 722 (2017); https://doi.org/10.1126/science.aai9081

[11] G. Niu, X. Guo, and L. Wang, J. Materials Chemistry A, 3, 8970 (2015); https://doi.org/10.1039/C4TA04994B

[12] J. Liu, Y. Wu, C. Qin, X. Yang, T. Yasuda, A. Islam, and L. Han, Energy & Environmental Science, 7, 2963 (2014); https://doi.org/10.1039/C4EE01589D

[13] W. Ke, G. Fang, J. Wan, H. Tao, Q. Liu, L. Xiong, P. Qin, J. Wang, H. Lei, G. Yang, M. Qin, X. Zhao, Y. Yan, Nature Communications, 6, 6700 (2015); https://doi.org/10.1038/ncomms7700

[14] L. X. Shi, Z. S. Wang, Z. Huang, W. E. I. Sha, H. Wang, and Z. Zhou, AIP Advances, 8, 025312 (2018); https://doi.org/10.1063/1.5021293

[15] F. Huang, Y. Wei, L. Gu, Q. Guo, H. Xu, D. Luo, S. Jin, X. Yang, Y. Huang and J. Wu, Energy Technology, 5, 1844 (2017); https://doi.org/10.1002/ente.201700437

[16] K. M. Boopathi, M. Ramesh, P. Perumal, Y. C. Huang, C. S. Tsao, Y. F. Chen, C. H. Lee, and C. W. Chu, J. Materials Chemistry A, 3, 9257 (2015); https://doi.org/10.1039/C4TA06392A

[17] C. W. Chen, H. W. Kang, S. Y. Hsiao, P. F. Yang, K. M. Chiang, and H. W. Lin, Advanced Materials, 26, 6647 (2014); https://doi.org/10.1002/adma.201402461

[18] R. Khan, S. Javed, M. Islam, IntechOpen. Pp.3-40, (2018); https://doi.org/10.5772/intechopen.74525

[19] L. Zheng, Y. H. Chung, Y. Ma, L. Zhang, L. Xiao, Z. Chen, S. Wang, B. Qu, and Q. Gong, Chemical Communications, 50, 11196 (2014); https://doi.org/10.1039/C4CC04680C

[20] M. L. Petrus, J. Schlipf, C. Li, T. P. Gujar, N. Giesbrecht, P. M. Buschbaum, M. Thelakkat, T. Bein, S. Hüttner, and P. Docampo, Advanced Energy Materials, 7, 1700264 (2017); https://doi.org/10.1002/aenm.201700264

[21] C. Eames, J. M. Frost, P. R. F. Barnes, B. C. O'Regan, A. Walsh and M. S. Islam, Nature Communications, 6, 7497 (2015); https://doi.org/10.1038/ncomms8497

[22] M. Grätzel, Nature Materials, 13, 838 (2014); https://doi.org/10.1038/nmat4065

[23] A. Kojima, K. Teshima, Y. Shirai, and T. Miyasaka, J. American Chemical Society, 131, 6050 (2009); https://doi.org/10.1021/ja809598r

[24] G. Giorgi, J. I. Fujisawa, H. Segawa, K. Yamashita, J. Physical Chemistry Letters, 4, 4213 (2013); https://doi.org/10.1021/jz4023865

[25] K. Mahmood, S. Sarwar, M. T. Mehran, RSC Advances, 7, 17044 (2017); https://doi.org/10.1039/C7RA00002B

[26] N. E. Courtier, G. Richardson, J. M. Foster, J. M., Applied Mathematical Modelling, 63, 329 (2018); https://doi.org/10.1016/j.apm.2018.06.051

[27] P. Vivo, J. K. Salunke, A. Priimagi, Materials, 10, 1087 (2017); https://doi.org/10.3390/ma10091087

[28] F. F. Targhi, Y. S. Jalili, F. Kanjouri, Results in Physics, 10, 616 (2018); https://doi.org/10.1016/j.rinp.2018.07.007

[29] D. Kiermasch, P. Rieder, K. Tvingstedt, A. Baumann, V. Dyakonov, Scientific Reports, 6, 39333 (2016); https://doi.org/10.1038/srep39333

[30] A. Guerrero, G. G.Belmonte, I. M. Sero, J. Bisquert, Y. S. Kang, T. J. Jacobsson, J. P. C. Baena A. Hagfeldt, J. Physical Chemistry C, 120, 8023 (2016); https://doi.org/10.1021/acs.jpcc.6b01728

[31] F. Maddalena, P. P. Boix, C. X. Yu, N. Mathews, C. Soci, S. Mhaisalkar, Charge Transport in Organometal Halide Perovskites. In: N. G. Park, M. Grätzel, T. Miyasaka, (eds) Organic-Inorganic Halide Perovskite Photovoltaics, Springer, Cham, pp.201-222, (2016); https://doi.org/10.1007/978-3-319-35114-8_8

[32] A. Todinova, L. C. Bernal, M. Salado, S. Ahmad, N. Morillo, J. Idígoras, J. A. Anta, ChemElectroChem, 4, 2891 (2017); https://doi.org/10.1002/celc.201700498

[33] H. Hu, B. Dong, W. Zhang, J. Materials Chemistry A, 5, 11436 (2017); https://doi.org/10.1039/C7TA00269F

[34] J. Chaudhary, S. Choudhary, C. M. S. Negi, S. K. Gupta, A. S. Verma, Physica Scripta, 94, 105821, (2019); https://doi.org/10.1088/1402-4896/ab2dc4

[35] J. Chaudhary, S. Choudhary, C. M. S. Negi, S. K Gupta, A. S. Verma, Semiconductors, 53, 489 (2019); https://doi.org/10.1134/S1063782619040067

[36] K. Harada, A. G. Werner, M. Pfeiffer, C. J. Bloom, C. M. Elliott, K. Leo, Phys. Rev. Letts., 94, 036601 (2005); https://doi.org/10.1103/PhysRevLett.94.036601

[37] A. Upadhyaya, C. M. S. Negi, A. Yadav, S. K. Gupta, A. S. Verma, Superlattices and Microstructures, 122, 410 (2018); https://doi.org/10.1016/j.spmi.2018.07.001

[38] C. H. Ji, K. T. Kim, S. Y. Oh, RSC Advances, 8, 8302 (2018); https://doi.org/10.1039/C8RA00730F

[39] L. Dou, Y. M. Yang, J. You, Z. Hong, W. H. Chang, G. Li, Y. Yang, Nature Communications, 5, 5404 (2014); https://doi.org/10.1038/ncomms6404

[40] A. Upadhyaya, C. M. S. Negi, A. Yadav, S. K. Gupta, A. S. Verma, Semiconductor Science and Technology, 33, 065012 (2018); https://doi.org/10.1088/1361-6641/aac066

[41] J. Dacuña, A. Salleo, Phys. Rev. B, 84, 195209 (2011); https://doi.org/10.1103/PhysRevB.84.195209

[42] Q. Dong, Y. Fang, Y. Shao, P. Mulligan, J. Qiu, L. Cao, J. Huang, Science, 347, 967 (2015); https://doi.org/10.1126/science.aaa5760

[43] Z. Zhang, W. Zheng, R. Lin, F. Huang, Royal Society Open Science, 5, 180905 (2018); https://doi.org/10.1098/rsos.180905

[44] S. R. Raga, Y. Qi, J. Physical Chemistry C, 120, 28519 (2016); https://doi.org/10.1021/acs.jpcc.6b11584

[45] N. Sharma, C. M. S. Negi, A. S. Verma, S. K. Gupta, J. Electronic Materials, 47, 7023 (2018); https://doi.org/10.1007/s11664-018-6629-3